UNDERSTANDING CHANGES AND DEFORMATIONS ON MULTI-TEMPORAL ROCK FACE POINT CLOUDS

M. Scaioni, M. Alba

Politecnico di Milano, Dept. B.E.S.T., via M. d'Oggiono 18/a, 23900 Lecco, Italy - e-mail: {mario.alba, marco.scaioni}@polimi.it

Commission III/2

KEY WORDS: Point Cloud, Change Detection, Deformation Monitoring, Terrestrial Laser Scanning, Digital Surface Analysis

ABSTRACT:

The paper outlines an approach to compare two digital surfaces of a rock face in order to extract geometric changes and deformations. The method requires the preliminary registration of each point cloud by using techniques typical of TLS. Then, point clouds are segmented in several regions, each of them referred to a plane; this task allows to interpolate all data to obtain a set of grid DEMs per epoch. Then each pair of corresponding DEMs are subtracted point-wise to obtain the ΔDEM of the differences along elevation. This is then processed along a three-step procedure. First possible systematic errors or low-frequency deformations are extracted by looking for a linear component. Secondly, the remaining ΔDEM is check against major changes, i.e. loss of material or vegetation growth. Finally, deformations of the cliff are enhanced by analyzing the mean displacement through the convolution with a square window applied to the ΔDEM filtered out from holes and bushes. This technique improves the original precision of each measured point, because deformation is evaluated as mean of a sample on the ΔDEM. The method has been tested so far on both synthetically generated and simple real data sets.

1 INTRODUCTION

Today the high potential of 3D surface reconstruction provided by Terrestrial Laser Scanning (TLS) has opened up many new prospects of application. Among these, *deformation monitoring* based on the comparison of multi-temporal point clouds is one of the most challenging. The advantage of this approach is relevant: geodetic monitoring techniques can achieve very precise measurements but limited to few control points, while point cloud analysis extends the observation to whole surfaces, including areas which usually are not investigated. In literature different experiences are reported, involving for the most applications to Geology, Civil and Building Engineering (Vosselmann and Maas, 2010). One of the common issues afforded by several authors is how to cope with uncertainty in point clouds, being this the bottle-neck of deformation measurement by TLS. Three main aspects contribute to the error budget, which is larger with respect to the standard monitoring techniques: precision of *intrinsic measurements*, point cloud *registration*, and *data modelling*. An interesting strategy that was adopted to overcome the problem of the measurement uncertainty is given by the so called *area-based* techniques. These make use of surfaces (planes or other regular shapes) interpolating the point clouds to be compared. This task might be performed on the whole object, when it features a known shape (Lindenbergh et al., 2005, Schneider, 2006, Gordon and Lichti, 2007), or on some parts of it (Lindenbergh and Pfeifer, 2005). In both cases, the object surface should be regular, like frequently occurs in the analysis of man-made structures. A higher degree of complexity is involved in the geological field, especially when dealing with deformation analysis of *rock faces*. Indeed, different applications were successfully carried out on terrain slopes and landslides, due to the fact the displacements to detect are very often larger than the accuracy of the adopted sensors (Abellán et al., 2006, Teza et al., 2007). When dealing with cliffs where the rockfall risk is relevant the problem becomes more complex, because the accuracy needed for failure forecasting is very often lower than the uncertainty of the adopted observations. A small number of papers were published so far on this subject, and no one presents an exhaustive and general approach. Interesting inputs can be found in (Abellán et al., 2009). Besides the problem of the required accuracy in data acquisition and modelling, ranging in the order of few cm up to 0.5 mm according to the size and the topography of the site, some further problems have to be tackled. Deformations might generally occur on an entire portion of a slope, or they might affect a local region only. The former requires to establish a stable *ground reference system* (GRS), calling for the use of high precision geodetic techniques. Alternatively, a comparison with external stable rock areas is needed, but this solution usually does not guarantee enough accuracy. The latter might be overcome by considering relative displacements between close regions. In addition, on rock faces vegetation can grow, and blocks can fall down between observation epochs, resulting in significant *major changes* on the surfaces where deformations occurred.

In this paper a method to perform a deformation analysis of a rock face is presented, accounting for both the detection of local major changes and widespread deformations. Examples of application to a synthetically generated dataset and to a simple real dataset are reported in Section 3.

2 A TECHNIQUE FOR THE COMPARISONS OF ROCK FACE SURFACE ALONG TIME

The basic concept that was followed here is to exploit the data redundancy of a point cloud to improve the precision of detectable deformations and changes. However, the application of this principle to rock faces is more complex than it is in case of man-made structures, due to the presence of irregular surfaces which prevent from interpolation with analytical functions, to possible major changes on point clouds, and to the millimetric precision required.

The full data processing workflow proposed and discussed in this paper is shown in Fig. 1. The method requires the preliminary acquisition and registration of each point cloud by using standard methods of the adopted sensor technology. Here the use of TLS is assumed, but 3D modeling through Photogrammetry could be also used, if enough accuracy and resolution are provided. Then, point-clouds are segmented into several 2.5D re-

gions, each of them referred to its own plane. This task allows to interpolate the raw data to obtain a grid DEM for each region. Considerations about scan georeferencing and preliminary filtering from vegetation are reported in (Alba et al., 2010). Hereafter, the processing is carried on by computing point-wise differences between both DEMs of the same region corresponding to different epochs. The ΔDEM achieved this way is then analysed along a three-step procedure. First, possible systematic effects or low-frequency deformations are extracted by looking for a linear component in the ΔDEM. If this component is statistically significant, it is removed from the dataset. Thus the ΔDEM is checked against *major changes*, i.e. loss of material or vegetation growth. Finally, deformations are looked for by analyzing the mean deformations computed on square windows of a few decimeter side, process that should theoretically improve the original precision of each point. Deformations are detected on the basis of statistical testing, which requires an estimate of the ΔDEM precision (see Par. 2.6.1).

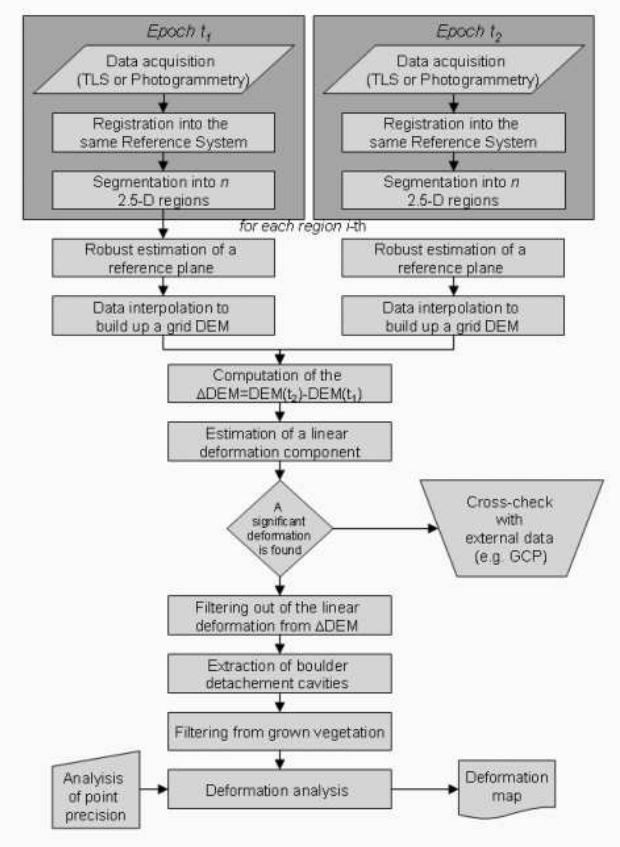

Figure 1: Workflow of the procedure for rock face deformation analysis.

2.1 Preliminary data processing

Deformation analysis is carried out on the basis of two datasets taken under the same operational conditions at epochs t_1 and t_2. Details about data acquisition planning and instruments can be found in Alba et al. (2005). At least one epoch data must be georeferenced into a GRS in order to align the z axis of the *project RS* (PRS) to the local plumb-line, and to refer data to the national mapping system. Indeed, in the geomorphological analysis these tasks are generally needed to define the spatial orientation of rock discontinuities. On the other hand, the use of GCPs to register point cloud at epoch t_2 into the same RS cannot be enough to obtain an accuracy suitable to detect deformations (Alba et al., 2009). An approach based on the relative scan coregistration by means of ICP algorithm might allow to improve the relative accuracy, even though it requires that stable parts are in the scene.
The technique that is currently implemented for the analysis of surfaces requires that both point clouds to be compared are resampled on a regular grid (DEM) established with respect to a reference plane. If the entire rock face under investigation has a complex morphology and cannot be referred to one plane only, a segmentation step is required to split up the whole dataset in smaller 2.5D regions. The method proposed by Roncella and Forlani (2005) is well suitable to this aim. This is based on a RANSAC segmentation technique requiring the definition of two input parameters: the maximum allowed distanced of a point from its reference plane, and the minimum number of points per region. In order to avoid different segmentations at two epochs, this procedure is applied to point cloud 1, and then the boundary of each region Reg_k is utilized to subdivide point cloud 2. Hereafter, each region Reg_k will be separately analysed; accordingly, the subscript index k will be omitted. A plane π is estimated by Least Squares on the basis of points belonging to a specific region only. Finally, data can be resampled to a grid lattice, whose resolution δ_{DEM} (from now on called 'DEM Unit'–DU) is very close to the one of the original data to avoid loss of information. Each Reg at epoch t gives rise to a surface that is described by a rectangular matrix DEM^t to be used as input for next processing steps.

2.2 Computation of the ΔDEM

The deformation of a cliff consists in the change of the shape of its surface, due to sliding of rock masses along discontinuities. Usually deformations are preliminary to rockfalls, whose magnitude can depend on several factors. Thus the deformation analysis of a cliff's surface surveyed at two or more epochs must comprehends two main stages. The first one is the *change detection* (*ChDet*), which is focused to find rocks that fell down between two observation epochs and to filter out the grown vegetation. Regions that are interested by these two processes must be excluded from the next stage of the analysis. This is represented by the *deformation analysis* (*DefAn*) aimed to locate the areas that were affected by shape deformations.
The first step before proceeding with both items is to compute a new matrix ΔDEM resulting from the difference of the two DEMs concerning the same region (Reg):

$$\Delta DEM^{12} = DEM^2 - DEM^1. \quad (1)$$

The *area-based* methods for deformation analysis which have been quoted in Section 1 make use of interpolations of the original point clouds. Unfortunately, this approach can't be directly applied to the problem discussed here because of irregular surfaces. In absence of deformations and changes, the ΔDEM evaluated from Eq. 1 should be flat and regular, so that an *area-based* technique could be applied to it. Theoretically, elevations $z(i,j)$ of the ΔDEM should be normally distributed as $N(0,\sigma_z^2)$, where σ_z is the std.dev. of each ΔDEM point along z. Both algorithms *ChDet* and *DefAn* will look for discrepancies with respect to this stochastic model.
On the other hand, the use of ΔDEM introduces the following drawbacks: (i) the computation of ΔDEM requires interpolation of the original point clouds, task that increases the correlation between points at the same epoch; (ii) the use of DEMs results in a low-pass filtering, with consequent loss of information; (iii) misalignment errors on both DEMs at epochs t_1 and t_2 might be emphasized when computing the ΔDEM.

2.3 Extraction of the low-frequency deformation

A first deviation from the assumption on stochastic model is due to the presence of a low-frequency component in the ΔDEM. This might originate from three possible grounds: residual georeferencing errors; instability of the RS; major deformations on the cliff (e.g. due to a global displacement of the whole slope). Understanding the meaning of a such component is a complex issue, requiring context-aware analysis and comparison between results obtained on other *Reg*s and with geodetic measurements. On the other hand, here the main task is to look for low-pass deformation, that currently is implemented as the estimation of a 3D plane $\delta z = ai + bj + c$ fitting the ΔDEM. Because some major changes might be in the ΔDEM, the estimation of the linear component is carried out first by using a robust approach (L1-norm). Secondly, the final estimation of the plane parameters $\hat{x} = [\hat{a}\ \hat{b}\ \hat{c}]^T$ is performed by standard Least Squares. A χ^2 test on the estimated sigma naught ($\hat{\sigma}_0^2$) allows to check if the linear model fit the data well or not. In case of good fit a further statistical testing on the significance of each element of the vector $\hat{x}$ is applied to decide if a low-frequency component is worthy to be removed or not. Estimated parameters which are retained to be significant are stored in the vector $\hat{x}_s$; otherwise, their place in $\hat{x}_s$ is put equal zero. Finally the estimated low-frequency component is subtracted from the ΔDEM:

$$z'(i,j) = z(i,j) - [i\ j\ 1] \cdot \hat{x}_s. \tag{2}$$

2.4 Change detection algorithm

The *major changes* on a rock face are for the most due to the detachment of boulders or to the vegetation growing. Both feature some specific characteristics that allow to recognize them, and some others that are undifferentiated. For example, rock falls result in a negative change on the ΔDEM, while vegetation gives rise to positive changes during its growth and negative when leaves fall. Furthermore, other material could accumulate on the cliff resulting in positive changes on the ΔDEM (e.g. a bird nest).

The procedure that is described here cannot actually account for all these factors, but it tries to extract information from the ΔDEM according to a set of basic rules. First of all, rock detachments can result only in negative changes (holes) on the ΔDEM. Moreover, only blocks of significant size deserve to be considered, because smaller size rocks are not relevant for geological analyses. Two thresholds have been introduced to recognize holes in the ΔDEM: the *min width* (w_{cav}) of a rock-mass which has detached; the *min depth* (δz_{cav}) of the resulting cavity.

On the other hand, some specific techniques exist to remove the vegetated areas before data processing (see Alba et al., 2009; 2010). This results in the fact that at this stage both original DEMs have been already filtered out from vegetation, apart some errors which might still remain. However, two thresholds are established to detect the vegetation growth only: the *min bush width* (w_{veg}); the *min bush growth* along z direction (z_{veg}). Conversely, when leaves fall, the resulting hole in the ΔDEM can be confused with a rock detachment. A final visual inspection of results can help in understanding errors, perhaps by texturing the DSM of the cliff by using RGB (or NIR) images.

The basic concept of *ChDet* algorithm is to perform an analysis of volumetric changes by considering relevant variations in the ΔDEM surface. We consider here an approach useful for both losses of material and vegetation growth, even though each of this could be further specialized (e.g. by considering local roughness, curvature, or by integrating further data like RGB and NIR images, laser intensity). The assumption made is that changes are much larger that data uncertainty and they can be detected by fixing suitable thresholds depending on the geomorphology of the cliff. The localization of holes is carried out along the two following phases.

2.4.1 Holes localization The convolution of ΔDEM with a square matrix **H** is computed to define the map of mean displacements **M** in the nearby of each point:

$$\mathbf{M} = \Delta\text{DEM} \otimes \mathbf{H} = \Delta\text{DEM} \otimes \frac{1}{w_{cav}^2}\mathbf{I}. \tag{3}$$

Secondly, each element i, j of **M** is tested to check if it belongs to a region of detachment (or growth):

$$\forall i,j \in \mathbf{M} \begin{cases} \mathbf{D}_{ij} = 1, & \text{when } \mathbf{M}_{ij} < \delta z_{cav} \\ \mathbf{D}_{ij} = 0, & \text{elsewhere.} \end{cases} \tag{4}$$

The matrix **D** maps all discovered holes in the ΔDEM. According to the smoothness of **M** w.r.t. ΔDEM, once adequate thresholds w_{cav} and δz_{cav} have been established, commission errors are very unlikely. On the other hand, small losses of material could not be detected, but usually they are not relevant.

2.4.2 Improvement of the holes contours To better define the contours of each cavity and to improve the accuracy of computed detached volumes, a further procedure has been applied. Indeed, errors in the classification of contours by linear filtering might be larger when the depth of the holes is deeper.

First of all, elements of matrix **D** classified as detachments are grouped into clusters of points belonging to the same hole. Under the hypothesis that no commission errors have been made, all clusters are held, even though they feature few members only. Then the largest cross-section d_i of each hole *i*-th is computed according to **D**. A square window $\mathbf{W}_i$ sizing $2d_i$-1 DU is extracted from the ΔDEM at corresponding elements. A *median filtering* is applied to $\mathbf{W}_i$. This task might result in the loss of the smallest cavities found during linear filtering described at Subsection 2.4.1, because of the robustness of the *median filter* of size $w_{cav} \times w_{cav}$. For this reason, only holes accounting for a minimum number of points $n = 0.5 \cdot w_{cav}^2 + 1$ hold. Indeed, *median filtering* is applied only to redefine contours of already extracted holes, not to look for new ones. Results of latest filtering are stored into a matrix $\mathbf{M}'$. Now the test (4) is applied again but considering $\mathbf{M}'$ instead of **M**. After the second classification, the contour is redefined and points with $\mathbf{D}(i,j) = 1$ clusterized newly. In Figure 2 is shown somehow the use of the *median filtering* preserves the edge of a cavity in a cliff.

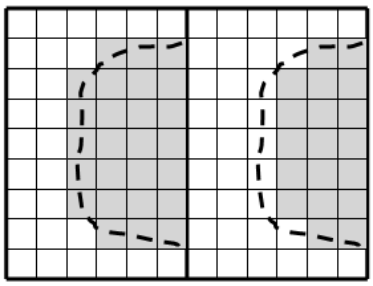

Figure 2: Differences in the definition of contours of a hole when applying a *linear* (left) or a *median filtering* (right)

2.4.3 Filtering out the grown vegetation The same procedure is then applied, if needed, to look for vegetation grown in the meanwhile of two observation epochs. Here only the localization stage is performed, because the precise volume of vegetation is

unwanted. The procedure described at Par. 2.4.1 is repeated by properly tuning the filtering process to detect grown areas and not holes. Results of detection are stored in a mapping matrix **V**.

2.5 Output map generation

Once the change detection stage is completed the final maps of detachments and of green areas can be plotted in 2D and can be projected on the original point cloud. Thank to a final clustering of points belonging to the same region, specific information (average diameter, volume, areas,...) on each of them can be exported and analysed into a GIS/CAD environment. Here other kinds of data available could be integrated, such as DEMs, orthoimages, vector data, geomorphological models and the like.
Because some errors might have occurred in either detachment and vegetation detection, some pixels belonging to one of these classes could not have been classified. These mistakes would influence the *DefAn* algorithm and then must be removed. To do this, elements in the mapping matrices that are around the borders of the already detected contours are excluded from the following analysis. This additional border has a width of 2 pixels around holes, and 5 pixels around vegetation spots, due to the major uncertainty in its determination. On the other hand, the exclusion of these elements is not expected to affect negatively the *DefAn* algorithm.

2.6 Deformation analysis

Here the approach for deformation measurement proposed in Lindenbergh and Pfeifer (2005) has been extended to irregular surfaces like rock faces. Points that are close among one another are expected to follow the same stochastic behavior and can be considered as a sample of a 1D random variable describing the elevations of the ΔDEM. Points that have been already classified in one of the map matrices are excluded from the *DefAn*. This requires to define a new map matrix **E**, whose elements are computed as:

$$\forall i, j: \quad \mathbf{E}_{ij} = \mathbf{D}_{ij} \cdot \mathbf{V}_{ij}. \tag{5}$$

The algorithm to detect deformations is described in the following items, with reference to Figure 3.

Parameter selection: the *width of the average window* (w_{def}) which defines each sample to compute deformations; the *spacing* Δw between adjacent sample windows; the *min number of valid points* (n_w) to be averaged. In this analysis these parameters play a fundamental role. In the experiments carried out so far the size of the averaging window was usually selected in the range 30-50 DU, while $\Delta w = w_{def}$.

Windowing of the ΔDEM: a given number of averaging windows is applied to the ΔDEM, according to parameters w_{def} and Δw; each of these will yield a deformation measurement $\delta z_w(r, s)$. From now on, the analysis is carried on a single averaging window a time.

Averaging into each window: $\delta z_w(r, s)$ is the mean of the valid points (n_{val}) into the corresponding averaging window; a point is valid according to its value in the mapping matrix **E**. To avoid of considering windows with too few valid points, the deformation analysis is carried on only if $n_{val} \geq n_w$.

Standard deviation of each sample mean: The std.dev. (σ_w) of the sample window (see Par. 2.6.1) is required to test the significance of each displacement $\delta z_w(r, s)$. The relevance of σ_w is obvious, because the lower is its value, the higher is the possibility to detect also very small deformations.

Testing the computed deformation: the H_0 hypothesis is that no deformation occurred (i.e. $\delta z_{0_w} = 0$); then the statistic $\xi = (\delta z_w(r, s) - \delta z_0)/\sigma_w \sim N(0, 1)$ is tested. Given a risk α and the corresponding critical value $\xi_{\alpha/2}$, H_0 is rejected if $|\xi| > \xi_{\alpha/2}$. It is then possible to fix in each window a minimum threshold for the acceptance of a significant deformation:

$$\delta z_{def} = \sigma_w \cdot \xi_{\alpha/2}. \tag{6}$$

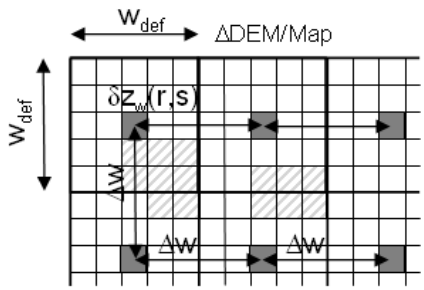

Figure 3: Example of averaging windows to computed the mean deformation $\delta z_w(r, s)$ on a square area on the ΔDEM; the zebra-hatched regions come from mapping matrix **E** and are excluded from the averaging.

2.6.1 Analysis of data precision Each DEM originates from points that can be considered uncorrelated between them after data acquisition (angles and ranges in case a TLS has been used). However, registration and modeling introduce correlations, which depend on the adopted interpolation technique. To keep into account correlations as well, an *empirical auto-correlation* function is computed on the ΔDEM (Crippa, 1991).
First of all, each element of the ΔDEM comes out from Eq. 1, where corresponding elements are uncorrelated. Its variance is then given by:

$$\sigma^2_{z_{\Delta DEM}} = \sigma^2_{z_{\Delta DEM^1}} + \sigma^2_{z_{\Delta DEM^2}} = 2\sigma^2_z, \tag{7}$$

where the std.dev. σ_z along z is the same at both epochs. The estimate of the variance of the sample mean is given as follows:

$$\sigma^2_w = \left(\frac{1}{n_{val}} + 2 \sum_{\substack{i=1,n_{val} \\ j=1,n_{val}}} \frac{1}{n^2_{val}} \rho_{ij} \right) \sigma^2_{z_{\Delta DEM}}, \tag{8}$$

where ρ_{ij} are correlations between elements i and j of the sample window. When computing Eq. 8, correlations can be roughly evaluated on the basis of the Euclidean distance between two points, by looking at the corresponding value on the *empirical auto-correlation* function.

3 APPLICATIONS

3.1 Application to a simulated dataset

The method presented here was initially tested on a synthetically generated dataset. The dataset 1 comes from the generation of two artificial surfaces of size 1000×1000 DU, corresponding to

an area of 20×20 m with DU=2 cm. the original std.dev. of points is assumed as $\sigma_z = 0.25$ DU. The first surface (epoch t_1) is flat, while the other one (t_2) presents every kind of changes and deformation that are dealt with in this paper:

- a global low-frequency deformation consisting on a shift along z whose mean value is half the size of the std.dev. of points;
- 4 cavities resulting from rock detachments featuring two different shapes (parallelepiped and semi-sphere), a footprint on the surface ranging from 7-21 DU, a depth from 2-8 DU;
- 3 areas with grown bushes with different shape and size: a parallelepiped (41×11×10 DU), a cylinder (21×51×11 DU), and a semi-sphere (R=20 DU); and
- a deformation consisting in a shift of 0.1 DU (2 mm) over a window of size $62,500$ DU^2 (i.e. 12.50 m^2).

In both DEMs a white noise was added up to z coordinates, and then the ΔDEM generated. Input thresholds and internal parameters are shown in Table 1. The low-frequency deformation was detected with no significant coefficients a and b of the estimated plane, according to the fact it consisted only on a shift along z direction; this was estimated with an error of 1.7%, corresponding to 0.1 mm. All the cavities and the vegetated areas have been correctly detected. The use of *median filter* in general improves border detection and then the area computation, even tough the results strongly depends on the size of the adopted search window.
The area of local deformation has been correctly detected. As can be seen in Table 1, two different sizes for the averaging window have been tried: 20 and 30 DU. The number of the averaged points in each sample window was 400 and 900, respectively, meaning that the precision of single points is theoretically 20-30 times better that of the sample mean. In reality, the contribute of correlations in Eq. 8 and the variance propagation (Eq. 7) when subtracting DEMs at different epochs reduce this increment of precision of 0.5 times. However, both configurations did not resulted in any major different outcomes. In Fig. 4 the evaluated deformations are reported when using a window size of 20 DU; in Fig. 5, red circles draw the position of the centers of windows where the displacement was evaluated as statistically significant.

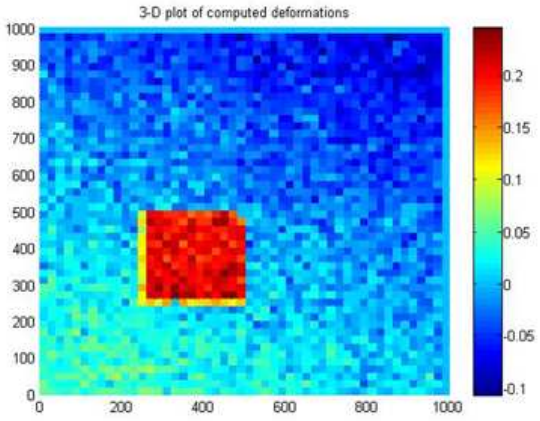

Figure 4: Detected deformation in dataset 1, where a search window of size 20 DU was adopted.

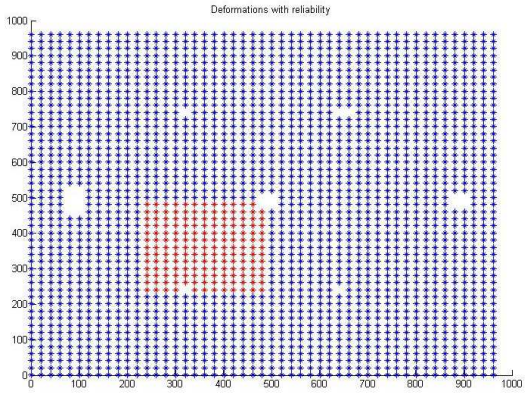

Figure 5: Results of the significance analysis on the deformation map shown in Fig. 4; red circles indicates the center of windows where displacement was tested as significant.

3.2 Application to a real dataset

After validating the algorithmic efficiency and the influence of individual input parameters on the dataset 1, the same algorithms have been tested on a real dataset 2. Data from a rock face collected at different times have been used. In Alba et al. (2009) problems concerning data acquisition, georeferencing, and vegetation filtering are discussed . The point clouds were acquired by a RIEGL LMSZ420i TLS with a linear resolution of 1.3 cm, and covering a rock face sizing 25×15 m. First of all, both point clouds acquired and georeferenced at different epochs were segmented (see Fig. 6) by the algorithm explained in Subsection 2.1, and after each region REG_k was analysed. For the dataset 2 only a region of 4.2×8.3 m with a strong presence of detachments was employed. Input thresholds and internal parameters are shown in Table 1.
Here the application of the *ChDet* algorithm successfully identified 5 detachments, for a total volume of 0.035 m^3, and 3 growths of vegetation for 0.002 m^3 (see Fig. 7). The results of the search for detachments were partially validated by recovering of some pieces of rocks corresponding to the detected holes in the ΔDEM (Fig. 8). The deformation analysis showed displacements of a few tenths of a millimeter, that however were not considered as statistically significant.

Example	1	1	2	2
Parameters	DU	cm	DU	cm
w_{cav}	4	8	2	10
δz_{cav}	2	4	1	5
w_{veg}	7	14	3	15
δz_{veg}	5	10	3	15
w_{def}	20/30	40/60	4	20
Δw	20/30	40/60	4	20
σ_z	±0.25	±0.5	±0.01	±0.5
Δ	1	2	1	5
$n_w(\%)$	90	90	90	90

Table 1: Input thresholds adopted in the processing of both simulated (1) and real (2) datasets.

4 CONCLUSIONS AND FUTURE WORK

In the paper a method for change detection and deformation analysis of multi-temporal digital surfaces of rock faces has been presented. The achievable results are a map of the fallen blocks,

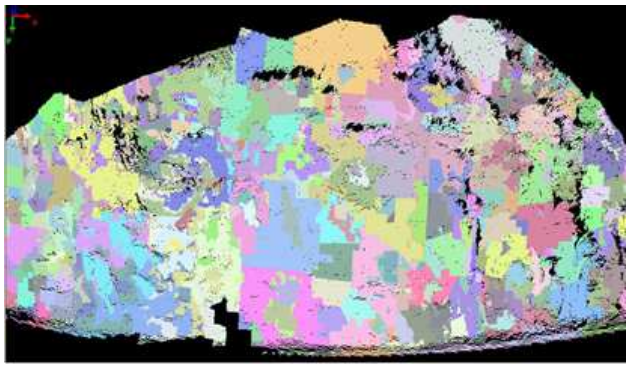

Figure 6: Results of the segmentation of the point cloud of dataset 2 at epoch t_1.

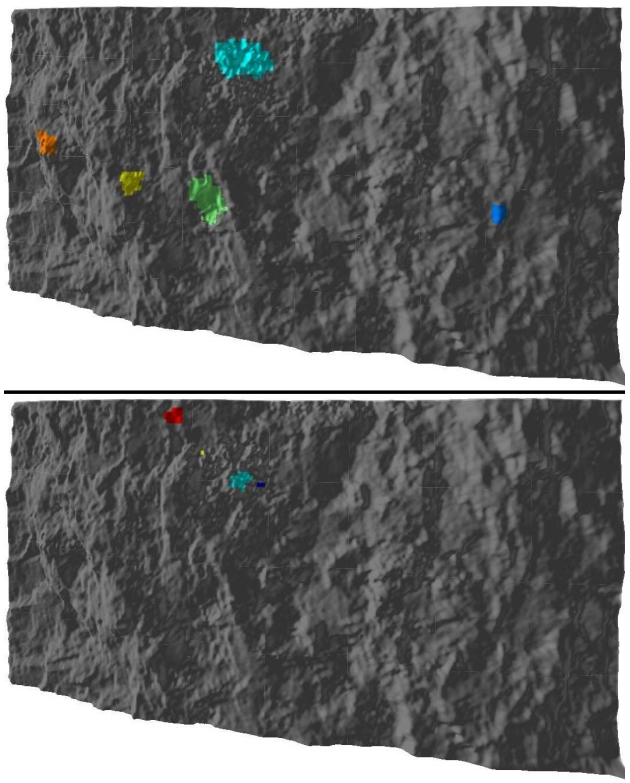

Figure 7: Results of *ChDet* analysis on the dataset 2: on the top image, the detected grown vegetation; on the bottom, the detected holes due to minor rockfalls.

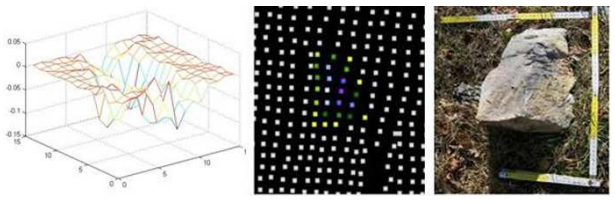

Figure 8: Image depicting a hole which was detected in dataset 2. On the right-most side the rock which corresponds to that hole is shown.

the removal of the grown vegetation, and a map of deformation. The process is highly automatic, a part from data preparation and interpretation. The availability of a technique for deformation measurements and rock detachment evaluation, integrated by the automatic extraction of dip and dip directions (Roncella and Forlani, 2005) will offer to experts on rockfall forecasting a powerful tool for an integrated analysis which today can be completely based on 3D surfaces reconstructed by TLS (or Photogrammetry).

The proposed method is based on the used of grid data (DEM). However, the DEM generation requires the interpolation of raw data, which introduces further uncertainty in the points. Further problems might arise when computing the difference (ΔDEM) between DEMs derived from surfaces captured at different epochs, e.g. due to misalignment errors or to lack of data. The improvement of the algorithms to work also with not-grid data is expected. Further improvements are required on the integration of results coming from adjacent regions (Reg), which so far are separately analysed. Furthermore, the introduction of FFT frequency analysis could help in modeling general and local deformation. The search for major changes (detachments and vegetation growth) might take advantage from the analysis of other parameters (local curvature, roughness, comparison with images).

Up until some tests were leaded on simulated and real datasets featuring a simple geometry, but more complicated configurations will be coped with in future to further prove the proposed methodology.

REFERENCES

Abellán, A., Jaboyedoff, M., Oppikofer, T. and Vilaplana, J., 2009. Detection of millimetric deformation using a terrestrial laser scanner: experiment and application to a rockfall event. Nat. Hazards Earth Syst. Sci. 9, pp. 365–372.

Abellán, A., Vilaplana, J. and Martínez, J., 2006. Application of a long-range terrestrial laser scanner to a detailed rockfall study at Vall de Nuria (Eastern Pyrenees, Spain). Eng. Geol. 2006(88), pp. 136–148.

Alba, M., Roncoroni, F. and Scaioni, M., 2009. Application of TLS for change detection in rock faces. In: IAPRSSIS, Vol. 38(3/W8), Paris, France, pp. 99–104.

Alba, M., Roncoroni, F. and Scaioni, M., 2010. Automatic detection of changes and deformation in rock faces by terrestrial laser scanning. In: IAPRSSIS, Vol. 39(5), Newcastle upon Tyne, UK, pp. 6 (on CD–ROM).

Crippa, B., 1991. Computational algorithms and optimal procedures for the digital terrain models production. Bollettino di Geodesia e Scienze Affini 1991(1), pp. 11–30.

Gordon, S. and Lichti, D., 2007. Modeling terrestrial laser scanner data for precise structural deformation measurement. J. Surveying Eng. 133(2), pp. 72–80.

Lindenbergh, R. and Pfeifer, N., 2005. A statistical deformation analysis of two epochs of terrestrial laser data of a lock. In: Proc. of the 7^{th} Conf. on Optical 3-D Measurement Techniques, Vol. 1, Vienna, Austria, pp. 61–70.

Lindenbergh, R., Pfeifer, N. and Rabbani, T., 2005. Accuracy analysis of the Leica HDS3000 and feasibility of tunnel deformation monitoring. In: IAPRSSIS, Vol. 36(3/W19), Enschede, The Netherlands, pp. 24–29.

Roncella, R. and Forlani, G., 2005. Extraction of planar patches from point clouds to retrieve dip and dip direction of rock discontinuities. In: IAPRSSIS, Vol. 36(3/W19), Enschede, The Netherlands, pp. 162–167.

Schneider, D., 2006. Terrestrial laser scanning for area based deformation analysis of towers and water dams. In: Proc. of 3^{rd} IAG Symp. on Deformation Measurements and Analysis/12^{th} FIG Symp. on Geodesy for Geotechnical and Structural Eng., Vol. 1, Baden, Austria, pp. 10 (on CD–ROM).

Teza, G., Galgaro, A., Zaltron, N. and Genevois, R., 2007. Terrestrial laser scanner to detect landslide displacement field: a new approach. Int. J. Remote Sens. 28(16), pp. 3425–3446.

Vosselmann, G. and Maas, H.-G., 2010. Airborne and Terrestrial Laser Scanning. 1^{st} edn, Whittles Publishing, Dunbeath, Caithness, Scotland, UK.